*Human Molecular Genetics*, 2019, Vol. 28, No. 24 4103–4112

**doi: 10.1093/hmg/ddz240**
Advance Access Publication Date: 19 October 2019
General Article

GENERAL ARTICLE

# *Elmod3* knockout leads to progressive hearing loss and abnormalities in cochlear hair cell stereocilia

Wu Li[1,10], Yong Feng[1,2,3,4], Anhai Chen[1,2], Taoxi Li[1,2,3], Sida Huang[1,2], Jing Liu[1,2], Xianlin Liu[1,2], Yalan Liu[1,2], Jiangang Gao[5], Denise Yan[6,7], Jie Sun[11], Lingyun Mei[1,2], Xuezhong Liu[1,6,7] and Jie Ling[1,8,9,*]

[1]Department of Otolaryngology, Xiangya Hospital, Central South University, Changsha, Hunan, China, [2]Province Key Laboratory of Otolaryngology Critical Diseases, Changsha, Hunan, China, [3]Hunan Jiahui Genetics Hospital, Changsha, Hunan, China, [4]National Clinical Research Center for Geriatric Disorders, Xiangya Hospital, Central South University, Changsha, Hunan, China, [5]School of Life Science and Key Laboratory of the Ministry of Education for Experimental Teratology, Shandong University, Jinan, Shandong, China, [6]Department of Otolaryngology, University of Miami Miller School of Medicine, Miami, FL, USA, [7]Dr. John T. Macdonald Foundation Department of Human Genetics, University of Miami Miller School of Medicine, Miami, FL, USA, [8]Institute of Molecular Precision Medicine, Xiangya Hospital, Central South University and Hunan Key Laboratory of Molecular Precision Medicine, Changsha, Hunan, China, [9]Hunan Key Laboratory of Animal Models for Human Diseases, School of Life Sciences, Central South University, Changsha, Hunan, China, [10]Department of Head and Neck Surgery, Hunan Cancer Hospital, The Affiliated Cancer Hospital of Xiangya School of Medicine, Central South University, Changsha, Hunan, China, and [11]The Eighth Affiliated Hospital, Sun Yat-sen University, Shenzhen, Guangdong, China

*To whom correspondence should be addressed at: Xiangya Hospital, Central South University, Changsha, Hunan 410008, China. Tel: +86731 84327246; Fax: +86731 84327246; Email: lingjie@sklmg.edu.cn

## Abstract

*ELMOD3*, an ARL2 GTPase-activating protein, is implicated in causing hearing impairment in humans. However, the specific role of *ELMOD3* in auditory function is still far from being elucidated. In the present study, we used the *CRISPR/Cas9* technology to establish an *Elmod3* knockout mice line in the C57BL/6 background (hereinafter referred to as *Elmod3*$^{-/-}$ mice) and investigated the role of *Elmod3* in the cochlea and auditory function. *Elmod3*$^{-/-}$ mice started to exhibit hearing loss from 2 months of age, and the deafness progressed with aging, while the vestibular function of *Elmod3*$^{-/-}$ mice was normal. We also observed that *Elmod3*$^{-/-}$ mice showed thinning and receding hair cells in the organ of Corti and much lower expression of F-actin cytoskeleton in the cochlea compared with wild-type mice. The deafness associated with the mutation may be caused by cochlear hair cells dysfunction, which manifests with shortening and fusion of inner hair cells stereocilia and progressive degeneration of outer hair cells stereocilia. Our finding associates *Elmod3* deficiencies with stereocilia dysmorphologies and reveals that they might play roles in the actin cytoskeleton dynamics in cochlear hair cells, and thus relate to hearing impairment.

**Received:** May 30, 2019. **Revised:** October 2, 2019. **Accepted:** October 3, 2019

## Introduction

Hearing loss (HL) is one of the most common sensory impairment in the human population. Approximately 1 in 850 infants is born with significant permanent hearing impairment annually, and the incidence rate may double by the age of 10 years (1). Moreover, auditory function progressively worsens with age. Age-related HL is the result of interactions between genetic predisposition and the aging process, including a variety of lifetime insults to the ear, which has a heritability approaching 55% in later life (2). For the vast majority of cases of hereditary HL, the mechanisms causing HL are not well understood at a molecular level.

It was first reported by Jaworek *et al*. in a large Pakistani family that the *ELMOD3* mutation (c.794 T > C; p.Leu265Ser) was responsible for autosomal recessive non-syndromic HL (3), and our group subsequently identified another *ELMOD3* mutation (c.512A > G; p.His171Arg) that segregates with non-syndromic progressive HL in a five-generation Chinese family in an autosomal dominant fashion (4). ELMOD3 exhibits ARL2 GTPase-activating protein (GAP) activity (3,5), yet little is known about its cellular function and molecular mechanism related to HL. A series of specific hearing disorders are caused by defects in the sensory hair cells in the inner ear, while sensory hair cells with mechanosensory hair bundle that protrudes from the apical surface of each hair cell can detect and amplify the softest sounds via hair cells mechanotransduction. The hair bundle deflections, caused by fluid movements that are induced by sound pressure, open mechanically gated transduction channels on the stereocilia tips (6). The resulting influx of cations depolarizes the hair cells and triggers neurotransmitter release, which initiates the transfer of auditory information to the central nervous system. Stereocilia are microvilli-derived mechanosensory organelles that are arranged in rows of graded heights on the apical surface of hair cells (7). Actin-based cytoskeleton within stereocilia of the hair bundles are essential to the mechano-electrical transduction process; hence, proper development and maintenance of these key structures are critical for hearing (8).

In this study, we established an *Elmod3* knockout (KO) mouse model using the CRISPR/Cas9 genome editing technology for further investigation of the auditory function affected by this gene. *Elmod3* deficiency leads to progressive HL in mice with the onset of 2 months of age and causes abnormalities in cochlear hair cells in the manner of shortening and fusion of the inner hair cell (IHC) stereocilia and progressive degeneration of the outer hair cell (OHC) stereocilia. The *Elmod3*$^{-/-}$ mice represent an animal model to assess the pathological abnormalities occurring within the cochlea in HL for understanding and potentially alleviating the progression of hair cell degeneration.

## Results

### Generation of *Elmod3* KO mice

CRISPR/Cas9 genome-editing technology was adopted to knock out the *Elmod3* gene in mice targeting on exon 6 (Supplementary Material, Fig. S1A and B), which produced a frameshift mutation with 277 bp deletion that led to an *Elmod3* null allele (Supplementary Material, Fig. S1C and D). To produce an *Elmod3* homozygous mutant, F0 male mice were bred to generate F1 mice. Then heterozygous (Het) mice were inbred to obtain homozygous mice. The newborn mice were genotyped using *Elmod3* KO-specific Polymerase chain reaction Polymerase chain reaction (PCR) primers (shown in Materials and Methods). The gene products of the wild-type (WT) allele should be 552 bp, while a 552 bp band and a 275 bp band were detected in Het mice and only a 275 bp band was observed in the homozygous KO mice (Supplementary Material, Fig. S1E–G). The genomic deoxyribonucleic acid (DNA) deletion leads to a frameshift mutation resulting in the generation of a premature termination codon at residue 149 (Supplementary Material, Fig. S1F). To confirm the expression of the deficiency of Elmod3 protein in KO mice, we performed western blot analysis on the cochlea extraction using anti-Elmod3 antibody. The Elmod3 protein expression in the cochlea was completely abolished in homozygous KO mice (Supplementary Material, Fig. S1H). And the frequencies of different genotypes of newborn mice were close to the expected Mendelian ratio (1:2:1); no sex bias was observed (data not shown). Taken together, the results consistently demonstrated the successful generation of *Elmod3* KO mice.

In addition, tracking analysis was performed to determine general phenotypic differences between WT, Het and KO mice. We only found that the body weights of WT and *Elmod3* KO mice were significant different. The homozygous KO mice exhibited decreases in body weight compared with the control groups of the same gender (Supplementary Material, Fig. S2).

### *Elmod3*$^{-/-}$ mice exhibit increased hearing thresholds across all frequencies and with normal vestibular function

To determine the potential importance of *Elmod3* for hearing, we first recorded auditory brainstem responses (ABR) to click and tone burst stimuli in anesthetized WT, *Elmod3*$^{+/-}$ and *Elmod3*$^{-/-}$ mice. In preliminary evaluation, no elevated ABR thresholds were found in any of 20 Het mice (*Elmod3*$^{+/-}$) at 2 months of age compared with WT mice; thus, we focused solely on *Elmod3*$^{-/-}$ mice compared with WT mice in subsequent analyses (Fig. 1A–C). In this study, the ABR testing was performed on mice from 1 to 5 months of age to assess the hearing thresholds with clicks and frequency-specific tone burst stimuli at four frequencies: 4, 8, 16 and 32 kHz. At the age of 1 month, ABR thresholds were not significantly different between *Elmod3*$^{-/-}$ and WT mice (Fig. 1A). However, the ABR thresholds shifted in *Elmod3*$^{-/-}$ mice compared with WT mice beginning from 2 months of age and lasted for the rest of time (Fig. 1B and C). The most significant difference occurred at 4, 8 and 16 kHz frequencies between 2-month-old WT and *Elmod3*$^{-/-}$ mice ($P < 0.001$) (Fig. 1B) and occurred at 8 and 16 kHz between 5-month-old WT and *Elmod3*$^{-/-}$ mice ($P < 0.001$) (Fig. 1C) by multi-frequency stimulation. Altogether, ABR testing results showed that the absence of *Elmod3* caused a moderate form of progressive HL in mice across all frequencies since 2 months old.

To determine whether the root cause of the sensorineural HL lies in impaired synaptic transmission, spiral ganglion (SG) neuron malfunction or a deficit in the active amplification process in the cochlea by OHCs motility, distortion products of the otoacoustic emissions (DPOAE) were performed (Fig. 1D–F). At the age of 1 month, 2f1-f2 DPOAE thresholds showed no significantly statistical differences in *Elmod3*$^{-/-}$ mice compared with WT mice (Fig. 1D). While at the age of 2 months, *Elmod3*$^{-/-}$ mice exhibited increased 2f1-f2 DPOAE thresholds compared with WT mice at this stimulation level and showed significantly statistical differences at 8, 12, 16 and 24 Hz ($P < 0.05$) (Fig. 1E). At the age of 5 months, *Elmod3*$^{-/-}$ mice exhibited greater significant differences of 2f1-f2 DPOAE thresholds across all frequencies from 4 to 32 Hz compared with WT mice ($P < 0.01$) (Fig. 1F). Altogether, the shifting of DPOAE thresholds indicated the reduction of the force coupled into the cochlear amplifier by OHCs motility.

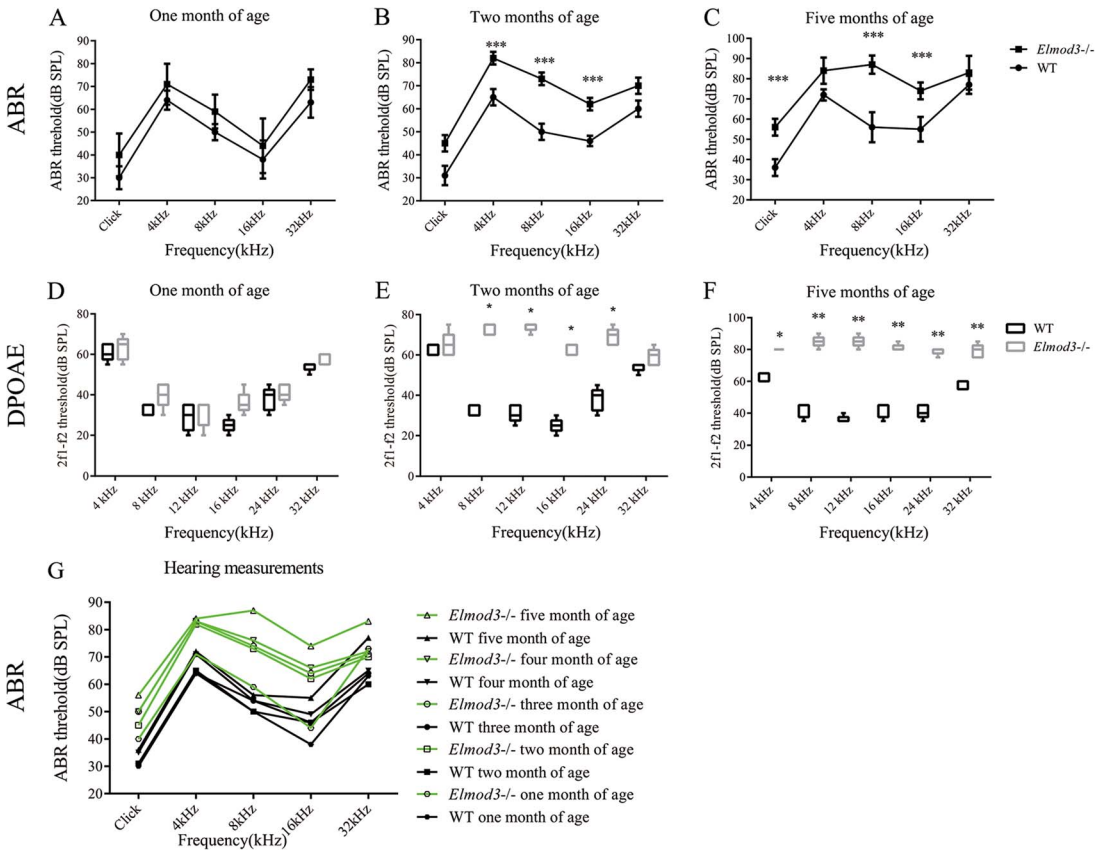


**Figure 1.** *Elmod3*$^{-/-}$ mice presented with a moderate and progressive form of HL. (**A**, **B** and **C**) ABR to click and tone burst stimuli at 4, 8, 16 and 32 kHz at different ages, 1 month of age (A), 2 months of age (B) and 5 months of age (C) in control (WT) and *Elmod3*$^{-/-}$ mice. (**D**, **E** and **F**) DPOAE at 4, 8, 12, 16, 24 and 32 kHz at different ages, 1 month of age (D), 2 months of age (E) and 5 months of age (F) in WT and *Elmod3*$^{-/-}$ mice. (**G**) ABR to click and tone burst stimuli at 4, 8, 16 and 32 kHz at different ages, from 1 month of age to 5 months of age combined together. Significant differences between WT and *Elmod3*$^{-/-}$ mice are indicated with *P*-values. $^{*}P < 0.05$, $^{**}P < 0.01$ and $^{***}P < 0.001$ (B and C, E and F). Error bars represent SE.

In addition, when combining the ABR thresholds of different age groups of mice together, it is obvious that the differences between WT and *Elmod3*$^{-/-}$ mice shifted greater along with aging (from 1 to 5 months old), especially occurring at 8 and 16 Hz, and the ABR thresholds were much higher in *Elmod3*$^{-/-}$ mice than in WT mice at all frequencies (Fig. 1G). These results indicated that the hearing impairment of *Elmod3*$^{-/-}$ mice progressed with aging.

In this study, no vestibular dysfunction was observed in any of the KO mice (data not shown). It is coincident with the clinical finding of patients carried with *ELMOD3* mutations in the two large HL families (3,4).

## *Elmod3*$^{-/-}$ mice show slight morphological change of cochleae and weaken F-actin cytoskeleton

To investigate whether the deficiency of *Elmod3* could cause the gross structure and morphological change of the cochlea in mice, thus resulting in hearing impairment, we examined the morphology of cochleae using hematoxylin–eosin (HE) staining. HE labeling of a cochlear section revealed an appeared normal gross morphology of the cochlea in *Elmod3*$^{-/-}$ mice compared with WT mice, but thinning and receding hair cells in the organ of Corti (OC) in *Elmod3*$^{-/-}$ mice at the age of 5 months (Fig. 2A and B).

Moreover, to find out whether the cellular morphological change of hair cells due to the defect of cytoskeleton, we performed immunostaining using anti-*myosin VIIa* antibody (pink) and phalloidin, an F-actin specific dye (green) (Fig. 2C and D). We found that green signals of F-actin were much more pronounced in WT mice (at postnatal day 30) compared with *Elmod3*$^{-/-}$ mice in many cell types in the cochlea, especially in hair cells. These results indicated a reduction of F-actin cytoskeleton formation in Elmod3 KO mice and therefore suggested that *Elmod3* is required for the proper organization of F-actin networks. In addition, phalloidin staining analysis (green) revealed that formation and maturation of stereocilia in OHCs and IHCs were relatively delayed in newborn *Elmod3*$^{-/-}$ mice (at postnatal 1 day) compared with the WT mice (Fig. 2E and F).

## Absence of *Elmod3* causes morphological defects of stereocilia in IHCs and OHCs

We further examined the morphology of stereocilia in IHCs and OHCs of *Elmod3*$^{-/-}$ mice and WT mice by scanning electron microscopy (SEM). At postnatal day 14, the micrographs of WT and *Elmod3*$^{-/-}$ mice resembled to each other (Fig. 3A and B). At the age of 5 months, stereocilia of OHCs were missing in both *Elmod3*$^{-/-}$ and WT mice with an increased frequency of losses in *Elmod3*$^{-/-}$ mice compared with WT mice (Fig. 3C and D). At the age of 2 months, when the KO mice began to show shifted hearing thresholds compared with WT mice, the gross micrographs of hair cells looked similar to each other for KO and WT mice (Fig. 4A and B). While when looking at IHCs, at the age of 2 months, stereocilia of IHCs were significantly short-

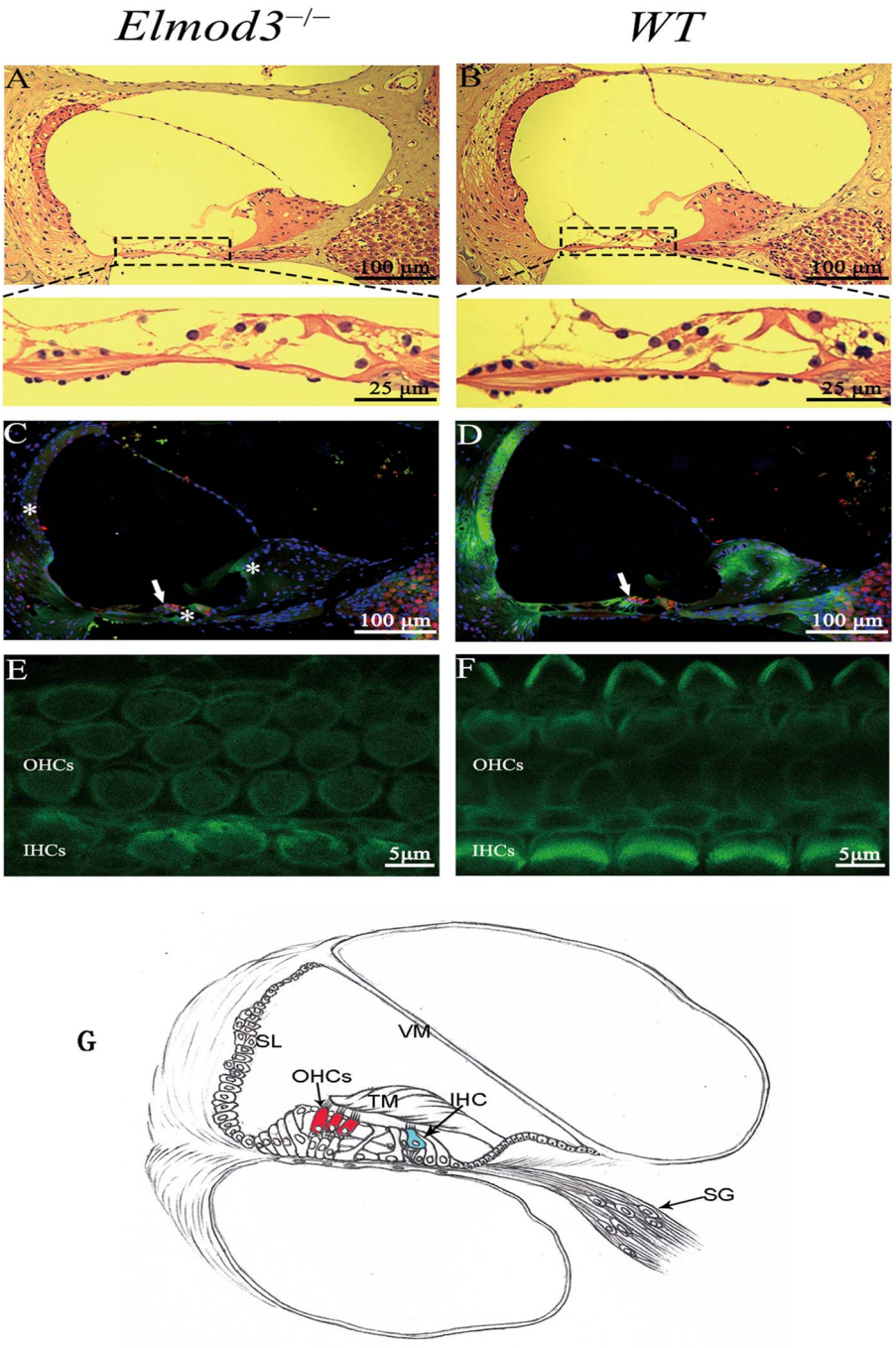


**Figure 2.** *Elmod3*$^{-/-}$ mice showed a slight morphology change of the OC and weakened F-actin cytoskeleton in the cochlea, especially in the OC. (**A** and **B**) Upper: low-magnification transverse view of the cochlea of adult mouse at postnatal 150 days with HE staining in *Elmod3*$^{-/-}$ mice (A) and WT mice (B). Scale bar:100 μm. Lower: high-magnification transverse view of the upper. Scale bar:25 μm. HE staining of cochlear sections revealed modest effects in the OC in *Elmod3*$^{-/-}$ mice with thinning and receding hair cells at 5 months old (A). (**C** and **D**) Low-magnification transverse view of the cochlea of adolescent mouse at postnatal 30 days with immunofluorescence staining in *Elmod3*$^{-/-}$ mice (C) and WT mice (D), stained by DAPI for nuclei (blue), *myosin VIIa* (pink) and phalloidin (green). Scale bar:100 μm. Green signals from phalloidin, an F-actin specific dye, were strikingly decayed in hair cells [with white arrow, in (C) and (D)], as well as in the OC, supporting cells, SG and SL [with white asterisk, in (D)]. (**E** and **F**) Confocal images of hair bundles in the surface of hair cells at postnatal 1 day newborn *Elmod3*$^{-/-}$ mice (E) and WT mice (F), stained with phalloidin (green). Scale bars: 5 μm. Green signals of stereocilia in OHCs and IHCs became quite weak and scattered in *Elmod3*$^{-/-}$ mice (E). (**G**) Schematic transverse view of the cochlea. Two types of auditory hair cells, one row of the IHCs and three rows of the OHCs, and surrounding supporting cells comprise the auditory epithelium (i.e. OC) and stereociliary bundles stretching from the tip surface of the hair cells in contact with the tectorial membrane.

ened in *Elmod3*$^{-/-}$ mice compared with the WT littermates (Fig. 4E and F). And by the age of 5 months, all IHCs exhibited noticeable degeneration of stereocilia with few IHCs completely lacking bundles in *Elmod3*$^{-/-}$ mice (Fig. 4G and H). And by the age of 5 months, *Elmod3*$^{-/-}$ mice showed a looser connection of stereocilia of OHCs hair bundles compared with WT mice (Fig. 4J–L), as well as increased losses of stereocilia in OHCs as mentioned above (Fig. 4I–K).

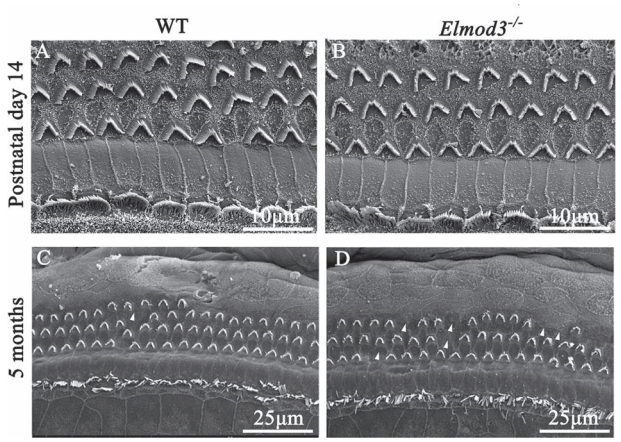


**Figure 3.** *Elmod3* deficiency did not cause significant hair cell losses. (**A** and **B**) Scanning electron micrographs of surface views of the whole-mount OC of WT mice (A) and *Elmod3*$^{-/-}$ mice (B) at postnatal 14 days assessed by SEM. The vast majority of hair cell bodies were present in the medial turn of the cochlea. WT and *Elmod3*$^{-/-}$ mice resembled each other at postnatal 14 days. Scale bars:10 μm. (**C** and **D**) Surface views of the OC of WT mice (C) and *Elmod3*$^{-/-}$ mice (D) at 5 months old assessed by SEM. The majority of IHCs were preserved in both *Elmod3*$^{-/-}$ and WT mice. And some stereocilia in OHCs were missing in WT and Elmod3 KO mice (white arrowheads) with an increased frequency of losses in *Elmod3*$^{-/-}$ mice (D) compared with the WT mice (C). Arrowhead pointed to the site of missing stereocilia in OHCs in the WT and *Elmod3*$^{-/-}$ mice (C and D). Scale bars: 25 μm.

### Arl2 selectively expressed in the cochlea and the expression level reduced in *Elmod3*$^{-/-}$ mice

Arl2 expression was detected in OHCs and IHCs, SG and spiral ligament (SL) of cochleae in WT mice (Fig. 5A). To determine whether the different genotypes differed in the Arl2 expression, western blot analysis was performed. Arl2 protein expression was reduced in *Elmod3*$^{-/-}$ mice compared with that of the WT mice at postnatal day 7 (Fig. 5F and G). This trend of reduced expression level of Arl2 between different genotypes in the OC was similar and consistent at the age of 1 month (Fig. 5B, C and H) and 5 months (Fig. 5D, E and I) based on the percentage of ARL2 positive cells. Additionally, in both WT and *Elmod3*$^{-/-}$ mice, we found that the percentage of Arl2 positive cells at the age of 5 months was reduced compared with that of 1 month olds (Fig. 5B–E).

## Discussion

Mutations in *ELMOD3* have been identified as causes of hearing impairment in human patients (3,4). In the present study, we reported the creation and characterization of a KO mouse model for *Elmod3* gene in order to understand the pathogenesis of hearing impairment associated with this gene. And we found that *Elmod3*$^{-/-}$ mice exhibited progressive loss of hearing and hair cells stereocilia morphology anomalies.

We measured hearing thresholds and examined hair cells stereocilia morphology in *Elmod3*$^{-/-}$ mice compared with WT mice. We found that *Elmod3*$^{-/-}$ mice exhibited significant HL beginning at the age of 2 months and progressed with age. Shortening and fusions of IHCs stereocilia and progressive degeneration of OHCs stereocilia were observed in *Elmod3*$^{-/-}$ mice. Shortened stereocilia in IHCs of *Elmod3*$^{-/-}$ mice were discovered at the age of 2 months and found to worsen in the later life of *Elmod3*$^{-/-}$ mice, which is consistent with the timing of the increased hearing threshold onset, and the hearing threshold was increased at 5 months of age in *Elmod3*$^{-/-}$ mice. Hair cells in the inner ear transduce auditory stimuli by deflection of their hair bundles, mechanically sensitive clusters of actin-rich stereocilia (9). Abnormality of these actin-based cytoskeleton structures in the hair cells, particularly those of stereocilia, is often the root cause of HL (10). The dysmorphic hair cell stereocilia indicates that Elmod3 is likely involved in the maturation or stability of inside structures in stereocilia.

The abnormal stereocilia phenotype observed in *Elmod3* KO mice hair cells is similar to that described in *Espin* (11,12), *Myosin XVa* (13), *Whirlin* (14,15) and *EPS8* (16) mutant mice, all of which exhibit stereocilia shortening and fusion. In contrast, striking stereocilia elongation and fusion were observed in KO mice of *Elmod1* (17), *Myosin VIIa* (18) and *Myosin VI* (19) mutant mice. *Elmod1* and *Elmod3* are paraloguous proteins, which both belong to the ELMOD family, known as ELMODs (20). *Elmod1* functions as a negative regulator of actin polymerization in mammalian hair cell stereocilia (21). Interestingly, pronounced abnormalities in IHCs stereocilia occurred in both *Elmod1* and *Elmod3* KO mice, while stereocilia length was reduced in *Elmod3*$^{-/-}$ mice but reversed in the *Elmod1* KO mice. Similarly, stereocilia length is reduced in mice lacking *Myosin XVa*, whereas *Myosin VIIa* and *Myosin VI* mutant mice exhibited elongated stereocilia, although all of the involved genes belong to the *Myosin* family.

In addition, no vestibular dysfunction was observed neither in *Elmod3*$^{-/-}$ mice nor in *ELMOD3*-mutation carriers in the previously reported families (3,4). Moreover, mutations in *ELMOD3* can cause dominant or recessive non-syndromic forms of deafness in humans, whereas in the present case, only homozygous *Elmod3*$^{-/-}$ mice manifest HL. Although mutations in *ELMOD3* genes have been associated with progressive HL in humans and mice, the pattern of inheritance difference between the two species may suggest that *ELMOD3* gene dosage may have a more significant effect in humans compared with mice.

By the way, severe hearing impairment was not observed in the already existing *Elmod3* KO mouse line, which described decreased lean body mass, a defect of cardiovascular and neurological systems as the sole finding (Mouse Genome Informatics, http://www.informatics.jax.org/; MGI ID: 6261063). In fact, HL with modest threshold changes usually cannot be detected without ABR and DPOAE tests.

ELMODs family are known as GAPs (5,20). GAPs regulate small GTP-binding proteins cycle between an inactive GDP-bound and an active GTP-bound form, as well as the rate of cycling. Moreover, GAPs are recognized as providing specificity to GTPase signaling (22). It is also known that ELMODs are GAPs regulating ARF-family small GTP-binding proteins (5,20,23). Among ELMODs, ELMOD1 exhibits the greatest GAP activity towards ARF6 (21), whereas ELMOD2 and ELMOD3 are GAPs that regulate ARL2 (3,23). ARL2 was considered as a higher-order signaling regulator for two essential cell functions in both mitochondrial fusion and microtubule dynamics due to different GAPs (24,25). Among a diverse group of ARF family GTPases that regulate organelle structure and membrane traffic, ARL2 is uniquely associated with regulation on microtubule dynamic polymerization (26). The ARL2–TBCD interaction is critical for proper maintenance of microtubule densities in cells and the TBCD–ARL2–$\beta$-tubulin trimer represents a functional complex whose activity is fundamental to microtubule dynamics (27). ARL2 provides a functional link between ARF family signaling pathways and the actin-based cytoskeletal architecture for stereocilia (28). In addition, Elmod3 exhibits mild ARL2 GAP activity and moderate symptoms in *Elmod3*-deficient mice potentially due to its

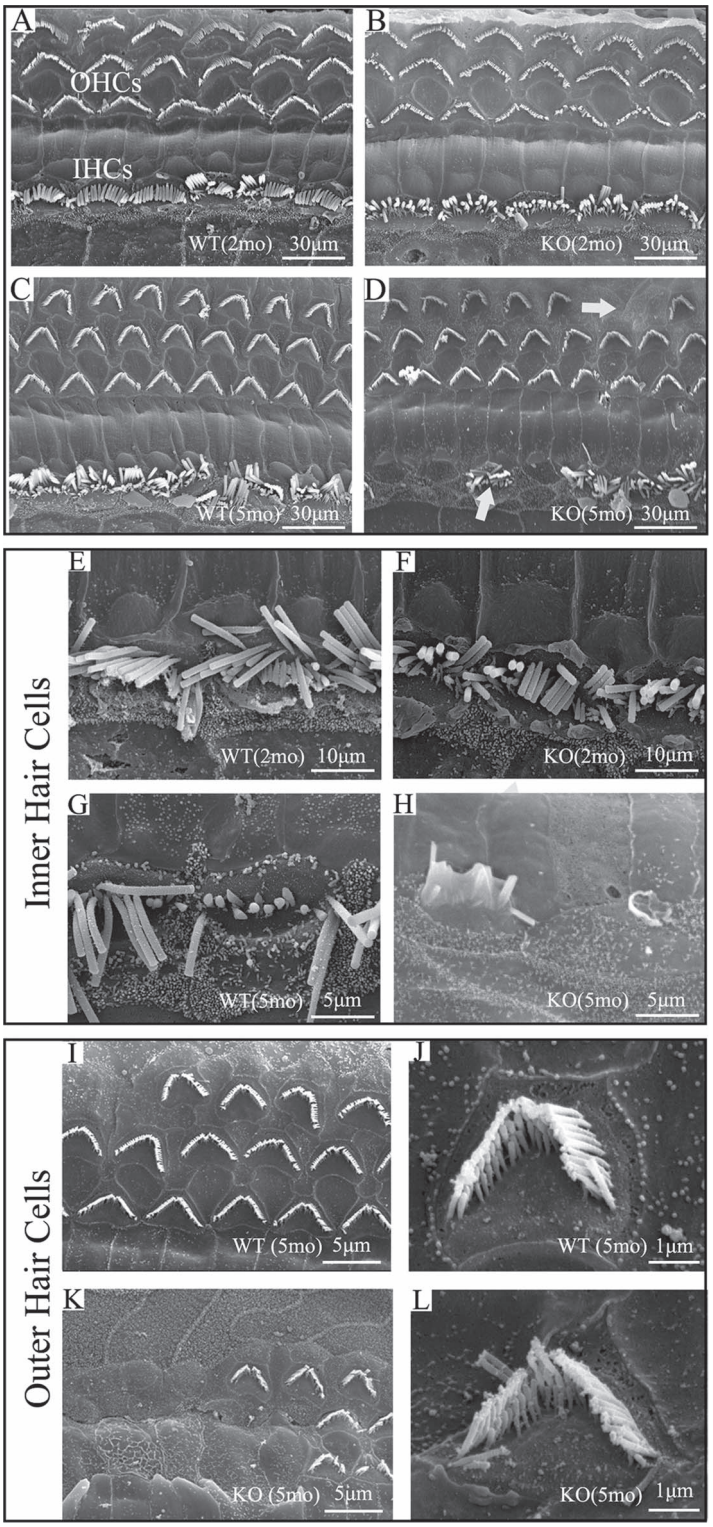


**Figure 4.** Absence of *Elmod3* causes morphological defects in mature stereocilia on hair cells. (**A**, **B**, **C** and **D**) Scanning electron micrographs of the surface of the OC in the medial turn of the cochlea of WT mice (A) and *Elmod3*$^{-/-}$ mice (B) at 2 months old, and WT mice (C) and *Elmod3*$^{-/-}$ mice (D) at 5 months old. Arrowhead pointed to the site of missing stereocilia in OHCs and IHCs (D). (**E**, **F**, **G** and **H**) Scanning electron micrographs of stereocilia in IHCs in 2-month-old WT mice (E) and *Elmod3*$^{-/-}$ mice (F), and in 5-month-old WT mice (G) and Elmod3$^{-/-}$ mice (H). (**I**, **J**, **K** and **L**) Low-magnification scanning electron micrographs of stereocilia in OHCs in 5-month-old WT mice (I) and *Elmod3*$^{-/-}$ mice (K), and high-magnification micrographs in WT mice (J) and *Elmod3*$^{-/-}$ mice (L). Scale bars are presented at the bottom of the picture.

low specific activity. Moreover, this study is the first report to describe the expression profiling of the ARL2 protein in the mouse cochlea as well as its reduction in expression level in the *Elmod3*$^{-/-}$ mice. Loss of Elmod3 and reduction in ARL2 expression level are likely responsible for the altered hair bundle morphology observed in *Elmod3*$^{-/-}$ mice.

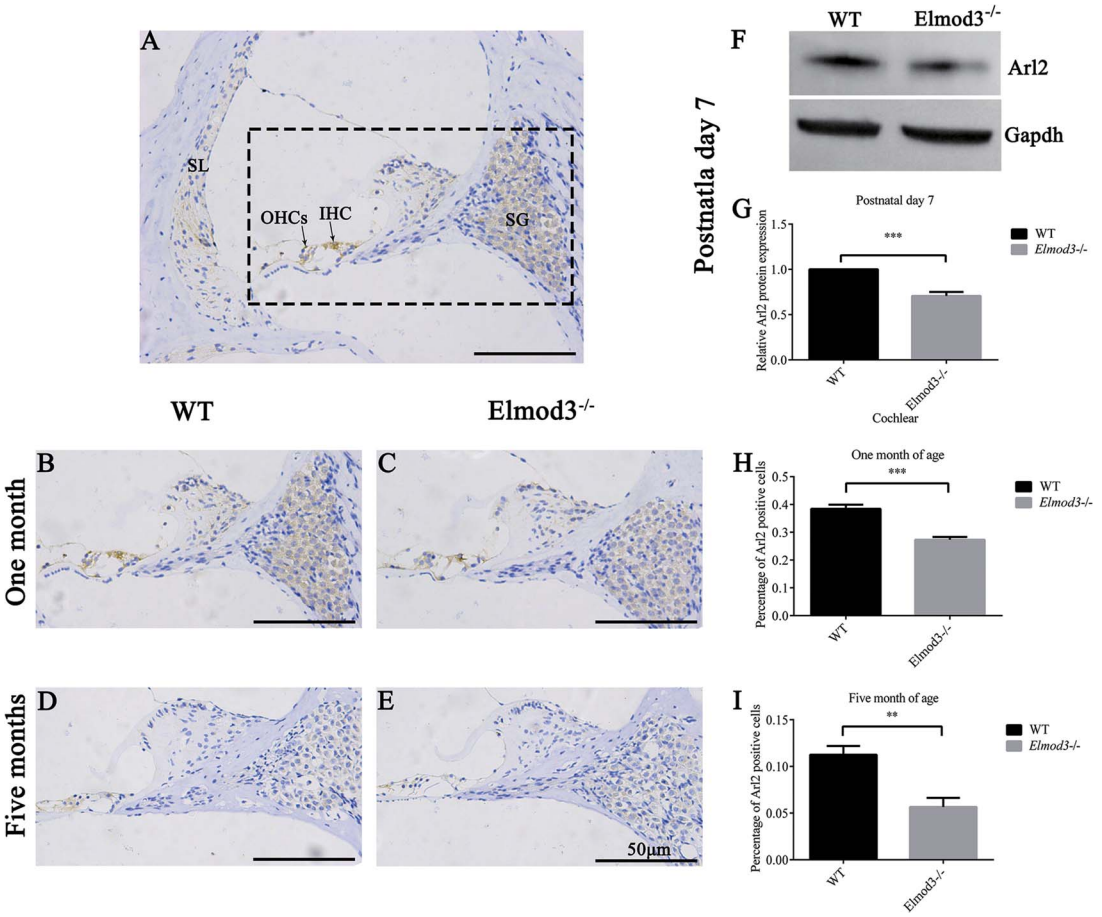


**Figure 5.** ARL2 is selectively expressed in the cochlea of mice and reduced ARL2 expression in the cochlea of *Elmod3*$^{-/-}$ mice. (**A**) Low-magnification transverse view of micrographs of 10 μm thin sections from the cochlea were incubated with the anti-ARL2 antibody and were then stained with hematoxylin for *in situ* expression analysis of ARL2 protein at 1 month of age in WT mice. ARL2 protein was expressed in OHCs and IHCs, SL and SG of the cochlea. Inside the dotted line rectangle in (A) was shown in (**B**), the micrograph from the same view of *Elmod3*$^{-/-}$ mice was shown in (**C**) and *in situ* expression analysis of ARL2 protein at 5 months of age in WT mice (**D**) and *Elmod3*$^{-/-}$ mice (**E**) were shown. Scale bars: 50 μm. A decreasing expression of ARL2 protein in the OC (B and C) at 5 months of age of mice (D and E) when compared with 1 month of age (B and C). Moreover, the ARL2 protein expression level significantly decreased in the *Elmod3*$^{-/-}$ mice. (**H** and **I**) The statistic diagram for (B) and (C), and (D) and (E), respectively, which is estimated by the percentage of ARL2 positive cells. Significant differences are indicated with *P*-values. $^{**}P < 0.01$ and $^{***}P < 0.001$ (H and I). SE represents error bars. (F) Western blotting assays of ARL2 protein expression level in postnatal 7 days mice cochlea of WT mice and *Elmod3*$^{-/-}$ mice. Expression level of ARL2 protein in *Elmod3*$^{-/-}$ mice were reduced compared with WT mice, and statistic diagram of (G) shown in (H). $^{*}P < 0.001$.

This study is the first *in vivo* report on *Elmod3*$^{-/-}$ mice. Our results revealed the progressive HL, stereocilia morphology anomalies and decreased expression of ARL2 in *Elmod3*$^{-/-}$ mice. A combination of many mechanisms acting in a concert might contribute to auditory dysfunction, which needs further elucidation, including refined structural and functional analyses of non-otic Elmod3-expressing cells in the KO mice. *ELMOD3* mutations lead to HL in humans, so these investigations may provide clues to help developing therapies to alleviate the effects of progressive hearing impairment involving hair cell stereocilia.

## Materials and Methods

### Ethics statement

All experimental procedures were approved by the Animal Ethics Review Committee of Xiangya Hospital, Central South University. All animal work was performed strictly in accordance with the Guide for Use of Laboratory Animals established by Xiangya Hospital.

### Mice

*Elmod3* KO mice on a C57BL/6 background were generated and maintained in Hunan Key Laboratory of Animal Models for Human Diseases of China. The *Elmod3* KO mice were generated by replacing exon 6 of the *Elmod3* gene, containing the start codon, by a neomycin resistance gene cassette, which results in a 277 bp deletion, including 87 bp deletion on the exon 6 and 191 bp lies in the neighboring intron. Genomic DNA was extracted from tails of the newborn pups. The genomic DNA fragment around the guide ribonucleic acid (RNA) target site was amplified by *Elmod3* KO-specific PCR primers as the following primer sets forward: 5'-GACCGTATCAGGCATGGCATGGTC-3' and reverse: 5'-AGGCTGTTCCCAGGGAGAAACCAAC-3'. F0 mice were bred to generate F1 mice. The DNA from the F1 offspring generation was sequenced to verify the mutation. F2 generation was obtained by intercrossing Het F1 offspring. The absence of full-length ELOMD3 protein was confirmed using a custom-designed polyclonal anti-ELMOD3 antibody (GenScript, Nanjing, China). Immunostaining of inner ear tissue in the present study showed a complete lack of Elmod3 in cochleae of homozygous animals.

### ABR measurements

ABR thresholds were measured to click and tone burst stimuli at frequencies of 4, 8, 16 and 32 kHz in a sound-isolated chamber using a Tucker–Davis Technologies (TDT) system workstation with SigGen32 software (Tucker–Davis Technologies Inc., Alachua, FL, USA). Briefly, mice were anesthetized with a ketamine/xylazine (18,2 mg/ml) solution (100/10 mg/kg body weight) and then placed on a soft pad. Subcutaneous electrodes were placed between the ears at the forehead for non-inverting, underneath the left external ear for inverting and the back near the tail for ground leads. ABR intensity series were collected with a descending series of stimulus levels in 5 dB steps beginning at 90 dB Peak equivalent sound pressure level (peSPL). In each age group, littermates composed of males and females were used—at least five animals per genotype. Three independent experiments were performed in triplicate.

### DPOAE measurements

Mice were anesthetized the same as described for ABR measurements. DPOAE response thresholds were tested as described previously (29). The DPOAE responding at diction frequency 2f1–f2 were measured with two primary tone frequencies (f1 and f2, with f2/f1 = 1.2 and f2 level 10 dB < f1 level) to predict auditory thresholds. DPOAE response thresholds were recorded at a range of frequencies (4, 8, 16, 24 and 32 kHz) within the acoustic microphone probe and the TDT system. Briefly, f1 and f2 emissions stimulated the cochlea and passed through a multifunction processor to a computer-controlled programmable attenuator, buffer amplifier and earphone. Stimuli were generated digitally, and the maximum level of stimuli for DPOAE was 90 dB Sound pressure level (SPL). 2f1–f2 DPOAE amplitude and the surrounding noise floor were then extracted. Hearing thresholds were defined as the averaged signals for each identified frequency tested and the comparison with the corresponding frequency in controls. Three independent experiments were performed in triplicate—the same as ABR measurements.

### Tissue processing and HE staining

Cochlear samples were fixed and decalcified. Samples were dehydrated by an ethanol series ranging from 30 to 100% and embedded in paraffin and then sectioned at a thickness of 10.0 μm. Samples were deparaffinized by an ethanol series ranging from 100 to 30%, and the OC was stained using HE. Images used for illustration were examined under light microscopy (Nikon YS100, Japan). Three independent experiments were done in triplicate and one sample per genotype was used each time.

### SEM

SEM of cochlear stereocilia was performed in ears from C57BL/6 WT mice and *Elmod3*$^{-/-}$ mice from postnatal 14 days, 2 months and 5 months of age. The temporal bones of mice were dissected. Cochleae were washed, fixed and decalcified, and the cochlear partition was then dissected in ice-cold phosphate buffered saline (PBS). Samples were mounted and sputter coated with gold. Stereociliary bundles were examined in the middle basal turns of the cochlea using a Hitachi S-4800 field emission scanning electron microscope (Hitachi S-4800, Japan). In each age group, one sample per genotype was used. Three independent experiments were done in triplicate.

### Preparation of protein extracts and western blot analysis

Mice were anesthetized and the cochlea were quickly removed from the skull and homogenized in ice-cold cell lysis buffer. The samples were lysed for 30 min on ice and centrifuged at 10 000 × *g* at 4°C for 30 min. The supernatant was then collected, and the protein concentration was measured using a bicinchoninic acid (BCA) protein assay kit (Thermo, USA). The samples were mixed with loading buffer, heated at 100°C for 5 min and stored at −20°C. Protein samples were separated by a 10% sodium dodecyl sulfate polyacrylamide gel and transferred onto a polyvinylidene difluoride (PVDF) membrane. The membrane was blocked in 5% non-fat dry milk in PBS-Tween (PBS-T) at room temperature for 1 h and incubated with primary antibodies at 4°C overnight. After washing with PBS-T (three times for 10 min each at room temperature), membranes were incubated with an anti-rabbit horseradish peroxidase-conjugated secondary antibody diluted in 5% non-fat dry milk in PBS-T at room temperature for 1 h. The membranes were then washed in PBS-T (three times for 10 min each), and bands were detected using an enhanced chemiluminescence (ECL) western blot detection kit (Thermo, USA). The following primary antibodies diluted in 5% bovine serum albumin were used: rabbit anti-Elmod3 (1 μg/ml, GenScript, China), rabbit anti-ARL2 (1:5000, Abcam, UK), rabbit anti-$\beta$-actin (1:5000, Sigma, USA) and rabbit anti-glyceraldehyde 3-phosphate dehydrogenase (GAPDH) (1:5000, Abcam, UK). The rabbit anti-Elmod3 polyclonal antibody was custom designed and produced by Genscript, China. GAPDH and $\beta$-actin were used as housekeeping genes to confirm equal sample loading.

### Immunohistology for ARL2 protein

The cochlea was quickly removed, fixed, decalcified and embedded in paraffin wax. Briefly, 10 μm thin sections were incubated in biotinylated anti-ARL2 antibody (1:250, Abcam, UK) as previously described. The percentage of ARL2 positive cells was counted based on specific brown-stained cells in the same field of vision.

### Immunofluorescence staining

For whole-mount immunostaining, the OC's sensory epithelium was isolated from the cochleae and divided into apical, middle and basal turn sections. Then, the samples were permeabilized in 0.5% Triton X-100 in PBS at room temperature for 15 min. The sections or cochlea samples were washed in PBS and then blocked in 10% goat serum in PBS at 37°C for 30 min. CytoPainter Phalloidin-iFluor 488 Reagent (Abcam, UK) was used to stain F-actin at 37°C for 30 min. Immunofluorescent images were collected using a confocal laser scanning microscope. For cochlear section immunofluorescence staining, cochlear sections were first treated with 0.5% Triton-X-100 (Sigma, USA) for 10 min and blocked with 7% normal goat serum (Sigma, USA) in PBS for 1 h followed by overnight incubation with anti-*myosin VIIa* antibody (10 μg/ml, Proteus, USA) at 4°C. Primary antibodies were detected with Cy3-conjugated goat anti-rabbit Ig antibody (0.35 μg/ml; Jackson ImmunoResearch Laboratories, USA) and CytoPainter Phalloidin-iFluor 488 Reagent (1:1000, Abcam, UK) at 37°C for 30 min. Sections were mounted with 4′ and 6-diamidino-2-phenylindole (DAPI) and photographed using the Olympus BX61 microscope with epifluorescence and cellSens Dimension software (Microscopes and Imaging Systems: Leica Microsystems MD500B). One sample per genotype was used each time. Three independent experiments were done in triplicate.

### Statistical analyses

All results were presented as the mean ± SD. Statistical comparisons of means among multiple groups were performed using two-way analysis of variance (ANOVA) followed by Student's *t*-test with a Bonferroni correction with the numbers of animal per genotype. For all tests, a value of $P < 0.05$ was considered to be statistically significant. GraphPad Prism 7 (GraphPad, San Diego, CA, USA) was used to calculate column statistics and compute *P*-values.

## Supplementary Material

Supplementary Material is available at *HMG* online.

## Funding

This work was supported by grants from the National Natural Science Foundation of China (81771023 and 81771024), the China Postdoctoral Science Foundation (2018M632999), the National Natural Science Foundation of Hunan (2019JJ50938), the Major State Basic Research Development Program of China (973 Program) (2014CB541702) and the National Institutes of Health/ National Institute on Deafness and Other Communication Disorders (R01DC005575 and R01DC012115).

## Acknowledgements

We thank the staff from Hunan Key Laboratory of Animal Models for Human Diseases of China for generating, maintaining and performing animal testing of mice in this study.

*Conflict of Interest statement*. None declared.

## References

1. Fortnum, H.M., Summerfield, A.Q., Marshall, D.H., Davis, A.C. and Bamford, J.M. (2001) Prevalence of permanent childhood hearing impairment in the United Kingdom and implications for universal neonatal hearing screening: questionnaire based ascertainment study. *The BMJ*, **323**, 536–540.
2. Gates, G.A., Couropmitree, N.N. and Myers, R.H. (1999) Genetic associations in age-related hearing thresholds. *Arch. Otolaryngol. Head Neck Surg.*, **125**, 654–659.
3. Jaworek, T.J., Richard, E.M., Ivanova, A.A., Giese, A.P., Choo, D.I., Khan, S.N., Riazuddin, S., Kahn, R.A. and Riazuddin, S. (2013) An alteration in ELMOD3, an Arl2 GTPase-activating protein, is associated with hearing impairment in humans. *PLoS Genet.*, **9**, e1003774.
4. Li, W., Sun, J., Ling, J., Li, J., He, C., Liu, Y., Chen, H., Men, M., Niu, Z., Deng, Y. *et al.* (2018) ELMOD3, a novel causative gene, associated with human autosomal dominant nonsyndromic and progressive hearing loss. *Hum. Genet.*, **137**, 329–342.
5. Ivanova, A.A., East, M.P., Yi, S.L. and Kahn, R.A. (2014) Characterization of recombinant ELMOD (cell engulfment and motility domain) proteins as GTPase-activating proteins (GAPs) for ARF family GTPases. *J. Biol. Chem.*, **289**, 11111–11121.
6. LeMasurier, M. and Gillespie, P.G. (2005) Hair-cell mechanotransduction and cochlear amplification. *Neuron*, **48**, 403–415.
7. Kitajiri, S., Sakamoto, T., Belyantseva, I.A., Goodyear, R.J., Stepanyan, R., Fujiwara, I., Bird, J.E., Riazuddin, S., Riazuddin, S., Ahmed, Z.M. *et al.* (2010) Actin-bundling protein TRIOBP forms resilient rootlets of hair cell stereocilia essential for hearing. *Cell*, **141**, 786–798.
8. Drummond, M.C., Belyantseva, I.A., Friderici, K.H. and Friedman, T.B. (2012) Actin in hair cells and hearing loss. *Hear. Res.*, **288**, 89–99.
9. Gillespie, P.G. and Muller, U. (2009) Mechanotransduction by hair cells: models, molecules, and mechanisms. *Cell*, **139**, 33–44.
10. Perrin, B.J., Strandjord, D.M., Narayanan, P., Henderson, D.M., Johnson, K.R. and Ervasti, J.M. (2013) Beta-actin and fascin-2 cooperate to maintain stereocilia length. *J. Neurosci.*, **33**, 8114–8121.
11. Rzadzinska, A., Schneider, M., Noben-Trauth, K., Bartles, J.R. and Kachar, B. (2005) Balanced levels of Espin are critical for stereociliary growth and length maintenance. *Cell Motil. Cytoskeleton*, **62**, 157–165.
12. Sekerkova, G., Richter, C.P. and Bartles, J.R. (2011) Roles of the *espin* actin-bundling proteins in the morphogenesis and stabilization of hair cell stereocilia revealed in CBA/CaJ congenic jerker mice. *PLoS Genet.*, **7**, e1002032.
13. Belyantseva, I.A., Boger, E.T. and Friedman, T.B. (2003) *Myosin XVa* localizes to the tips of inner ear sensory cell stereocilia and is essential for staircase formation of the hair bundle. *Proc. Natl. Acad. Sci.*, **100**, 13958–13963.
14. Kikkawa, Y., Mburu, P., Morse, S., Kominami, R., Townsend, S. and Brown, S.D. (2005) Mutant analysis reveals *whirlin* as a dynamic organizer in the growing hair cell stereocilium. *Hum. Mol. Genet.*, **14**, 391–400.
15. Mburu, P., Mustapha, M., Varela, A., Weil, D., El-Amraoui, A., Holme, R.H., Rump, A., Hardisty, R.E., Blanchard, S., Coimbra, R.S. *et al.* (2003) Defects in *whirlin*, a PDZ domain molecule involved in stereocilia elongation, cause deafness in the whirler mouse and families with DFNB31. *Nat. Genet.*, **34**, 421–428.
16. Zampini, V., Ruttiger, L., Johnson, S.L., Franz, C., Furness, D.N., Waldhaus, J., Xiong, H., Hackney, C.M., Holley, M.C., Offenhauser, N. *et al.* (2011) *EPS8* regulates hair bundle length and functional maturation of mammalian auditory hair cells. *PLoS Biol.*, **9**, e1001048.
17. Johnson, K.R., Longo-Guess, C.M. and Gagnon, L.H. (2012) Mutations of the mouse ELMO domain containing 1 gene (Elmod1) link small GTPase signaling to actin cytoskeleton dynamics in hair cell stereocilia. *PLoS One*, **7**, e36074.
18. Prosser, H.M., Rzadzinska, A.K., Steel, K.P. and Bradley, A. (2008) Mosaic complementation demonstrates a regulatory role for *myosin VIIa* in actin dynamics of stereocilia. *Mol. Cell. Biol.*, **28**, 1702–1712.
19. Avraham, K.B., Hasson, T., Steel, K.P., Kingsley, D.M., Russell, L.B., Mooseker, M.S., Copeland, N.G. and Jenkins, N.A. (1995) The mouse Snell's waltzer deafness gene encodes an unconventional *myosin* required for structural integrity of inner ear hair cells. *Nat. Genet.*, **11**, 369–375.
20. East, M.P., Bowzard, J.B., Dacks, J.B. and Kahn, R.A. (2012) ELMO domains, evolutionary and functional characterization of a novel GTPase-activating protein (GAP) domain for ARF protein family GTPases. *J. Biol. Chem.*, **287**, 39538–39553.
21. Krey, J.F., Dumont, R.A., Wilmarth, P.A., David, L.L., Johnson, K.R. and Barr-Gillespie, P.G. (2018) ELMOD1 stimulates ARF6-GTP hydrolysis to stabilize apical structures in developing vestibular hair cells. *J. Neurosci.*, **38**, 843–857.
22. Bos, J.L., Rehmann, H. and Wittinghofer, A. (2007) GEFs and GAPs: critical elements in the control of small G proteins. *Cell*, **129**, 865–877.

23. Bowzard, J.B., Cheng, D., Peng, J. and Kahn, R.A. (2007) ELMOD2 is an Arl2 GTPase-activating protein that also acts on ARFs. *J. Biol. Chem.*, **282**, 17568–17580.
24. Myers, K.R. and Casanova, J.E. (2008) Regulation of actin cytoskeleton dynamics by ARF-family GTPases. *Trends Cell Biol.*, **18**, 184–192.
25. Francis, J.W., Turn, R.E., Newman, L.E., Schiavon, C. and Kahn, R.A. (2016) Higher order signaling: ARL2 as regulator of both mitochondrial fusion and microtubule dynamics allows integration of 2 essential cell functions. *Small GTPases*, **7**, 188–196.
26. Al-Bassam, J. (2017) Revisiting the tubulin cofactors and Arl2 in the regulation of soluble alphabeta-tubulin pools and their effect on microtubule dynamics. *Mol. Biol. Cell*, **28**, 359–363.
27. Francis, J.W., Newman, L.E., Cunningham, L.A. and Kahn, R.A. (2017) A trimer consisting of the tubulin-specific chaperone D (TBCD), regulatory GTPase ARL2, and beta-tubulin is required for maintaining the microtubule network. *J. Biol. Chem.*, **292**, 4336–4349.
28. Stephen, L.A., Elmaghloob, Y. and Ismail, S. (2017) Maintaining protein composition in cilia. *Biol. Chem.*, **399**, 1–11.
29. Steigelman, K.A., Lelli, A., Wu, X., Gao, J., Lin, S., Piontek, K., Wodarczyk, C., Boletta, A., Kim, H. and Qian, F. *et al.* (2011) Polycystin-1 is required for stereocilia structure but not for mechanotransduction in inner ear hair cells. *J. Neurosci.*, **31**, 12241–12250.